Proceedings Paper:

Khan, Z.U., O'Farrell, T. and Ford, K.L. orcid.org/0000-0002-1080-6193 (2023) Direct IF sampling receivers for 5G millimeter-wave communications systems. In: 2023 IEEE 34th Annual International Symposium on Personal, Indoor and Mobile Radio Communications (PIMRC) Proceedings. 2023 IEEE 34th Annual International Symposium on Personal, Indoor and Mobile Radio Communications (PIMRC), 05-08 Sep 2023, Toronto, ON, Canada. Institute of Electrical and Electronics Engineers (IEEE) , pp. 1-5. ISBN 9781665464840

https://doi.org/10.1109/pimrc56721.2023.10293990

Direct IF Sampling Receivers for 5G Millimeter-Wave Communications Systems

Zia Ullah Khan
Dept. Electron. and Electr. Eng.
University of Sheffield
Sheffield, UK
z.u.khan@sheffield.ac.uk

Timothy O'Farrell, Snr Member, IEEE
Dept. Electron. and Electr. Eng.
University of Sheffield
Sheffield, UK
t.ofarrell@sheffield.ac.uk

Kenneth L. Ford, Snr Member, IEEE
Dept. Electron. and Electr. Eng.
University of Sheffield
Sheffield, UK
l.ford@sheffield.ac.uk

***Abstract*—Reducing receiver complexity and power consumption are important design goals in fifth-generation (5G) millimeter-wave (mm-wave) communications systems. One approach for achieving these goals is to employ direct intermediate frequency (IF) sampling at sub-Nyquist rates in a superheterodyne receiver architecture using digital downconversion of the IF signal. This paper presents original measured results characterizing in detail the signal-to-noise-ratio (SNR), error vector magnitude (EVM), and block error rate (BLER) performances of a direct IF subsampling mm-wave receiver with subsampling rate as a parameter. A software-defined radio (SDR) receiver using direct IF subsampling was implemented in a 28GHz, beamforming, over-the-air (OTA), hardware-in-the-loop (HWIL), SDR testbed using a 2.52 GHz IF. For a quadrature phase shift keying (QPSK) modulated long-term evolution (LTE) signal subsampled at 500 MHz, a small SNR penalty of ≈3dB at 5% BLER was obtained over a 10 GHz Nyquist sampling benchmark.**

***Index Terms*—Direct sampling, sub-Nyquist sampling, software-defined radio, 4G and 5G, millimeter-wave receiver**

I. Introduction

Fifth-generation wireless networks use higher carrier frequencies into the mm-wave region to support increased peak data rates and area capacity [1], [2]. Using mm-waves introduces additional challenges regarding receiver design, such as integrating various wireless devices that use distinct wireless standards into one cohesive system [3]. Realizing such units with conventional receiver architectures puts stringent requirements on the RF front-end and the analog-to-digital converters (ADCs), with increased count and power consumption of RF components [4], [5]. To overcome these obstacles, it is desirable to develop flexible, low-cost software-defined radio receivers that process more complex RF functionality in the digital domain [6], [7].

By using direct RF sampling to digitize the RF signal as soon as possible after the antenna, the software-defined radio (SDR) technique could provide the flexibility and cost reduction sought [8]–[10]. This comes at the cost of more demanding specifications and requirements for the ADC (e.g., high sampling rate, large analog input bandwidth, high power consumption, low dynamic range, reduced linearity, and lack of filtering agility) [11]. These requirements become more challenging when the mm-wave band is considered. ADCs using direct RF sampling in the mm-wave band (e.g. at 28 GHz) have significant cost and commercial availability constraints. Custom ADCs with up to 250 GSa/s are used in test and measurement equipment but they are not commercially accessible for use in generic mm-wave receivers. To the best of the authors' knowledge, commercially available state-of-the-art ADCs for generic applications have maximum sampling rates of up to 10 GSa/s and maximum analog input bandwidths of up to 8 GHz [12], [13]. Such ADCs exhibit power consumption in the order of watts.

A practical alternative to the mm-wave direct RF sampling receiver architecture is the direct IF sampling receiver, which downconverts the RF signal in a single mixer stage to a non-zero IF. The IF signal is directly digitized for signal processing using an ADC. By selecting an IF below 6GHz, a large range of commercial off-the-shelf (COTS) ADCs are readily available [14]. In [15] a SISO OTA communication link using direct IF sampling is demonstrated for a 64-QAM signal. A D-band RF signal at 159.4 GHz is downconverted to a 5GHz IF and subsequently direct IF sampled. The authors only demonstrate the system without disclosing the sampling design used (i.e., the ADC sampling rate or bit resolution) or providing an experimental characterization of the system performance. Losses due to sampling are not reported nor is an indication of the optimum sampling rate identified.

Sampling the bandpass IF signal at sub-Nyquist rates (i.e., subsampling) admits ADCs with low power consumption and high bit resolutions. The choice of the subsampling rate depends on several system parameters, in particular, the out-of-band noise floor and the IF bandpass filter (BPF) bandwidth, which determine the overall noise power after noise aliasing or folding. As mathematical analysis of the impact of the noise folding process on system performance is protracted, research based on the experimental characterization of SNR, EVM, and BLER has been more commonly used to design receivers. In [6] and [16], the authors investigate direct RF sampling and subsampling techniques in sub-6 GHz receivers, whereas no results of comparable experimental characterization exist for mm-wave receivers, including superheterodyne receivers.

The Xilinx Radio Frequency System on Chip (RF-SoC) technology combines programmable digital fabrics with high-speed ADCs/DACs on the same chip, enabling real-time Direct

IF sampling receivers [17]–[20]. The latest RF-SoCs support up to 16 ADCs/DACs with input analogue bandwidth of 6 GHz and ADC sampling frequency of 6 GSa/s. In [21], RFSoC technology has been utilized and frequency down conversion is performed from RF (28GHz) in one stage but direct conversion receivers are employed at the IF stage.

In [22], a direct subsampling receiver design is proposed for Ka-band applications using a sample and hold amplifier (SHA). The receiver performance is evaluated for the SHA only omitting the system characterized. In [23], a direct RF subsampling receiver model for the Ka-band is investigated for a high throughput satellite scheme but only the noise folding model is evaluated considering the roll-off rate of the anti-aliasing filter. There is no analysis for different subsampling rates and no assessment of overall system performance for a candidate transmission signal.

This paper presents original measured results for direct IF sampling and subsampling receivers for a SISO OTA 5G mm-wave communication link. For characterization, a 20 MHz LTE signal with QPSK digital modulation is first upconverted to 28 GHz before transmission over the air. At the receiver, the 28 GHz signal is downconverted to the IF signal using a single-stage downconversion mixer, and then presented for direct IF sampling. Direct IF sampling is performed at both Nyquist and sub-Nyquist sampling rates. The system performance is evaluated through the SNR, constellation EVM, and LTE system block error rate (BLER). The receiver power penalty as measured at the ADC input is identified for different sub-sampling rates corresponding to 3GPP benchmarks of 17.5% EVM for QPSK modulation, 5% BLER and 95% throughput.

II. System Design Description

The schematic diagram of a SISO OTA communication link with a direct IF sampling receiver is shown in Fig. 1. The NI PXI 5791 RF signal transceiver is employed in the test setup working together with the NI PXIe 7975R FPGA module for baseband signal processing. The NI-5791 provides the frequency up-conversion and down-conversion from the baseband signal to the intermediate frequency (IF). It has an independent onboard local oscillator (LO) for both RF input and RF output with frequency coverage from 200 MHz to 4.4 GHz. An LTE 20 MHz baseband (BB) signal is generated using the LabView-based LTE Application Framework, then the BB signal is converted to an analog signal, up-converted to the IF frequency of 2.52 GHz, and amplified utilizing the NI-5791 onboard digital to analog converters (DACs), frequency up-conversion unit, and amplifier [24].

For transmission in the mm-wave band, the IF transmitted signal from the NI 5791 is up-converted into the mm-wave band (to 28 GHz) using a frequency up-conversion unit, named UD (upconversion/downconversion) Box [25] (see schematic in Fig. 1). A bandpass filter (BPF) is employed after the frequency up-conversion to suppress any signals at the image frequency, LO leakage, and other unwanted signals. The BPF is a Mini-Circuits component [26], with a passband from 26.5 GHz to 29.5 GHz and a passband insertion losses of 0.75 dB

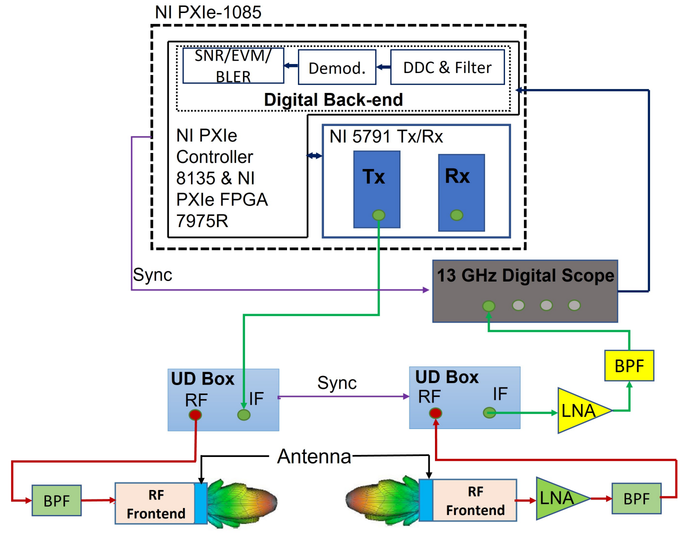

Fig. 1: Schematic for the SISO direct IF sampling transceiver.

[26]. The active phased array (consisting of a beamformer, amplifiers, and planar antenna array) is employed after the BPF filter. The 1×4 beamformer is set in the transmit (Tx) mode, for Line of Sight (LoS) communication between the transmit and receive antenna arrays. The transmit beamformer incorporates power amplifiers in the RF chain with a maximum power gain of 18 dB per branch at 28 GHz [27]. The employed planar antenna array consists of four linear arrays. Each linear array, consisting of 4 patch-antenna elements, has a realized maximum gain of ≈9 dBi in the broadside direction.

The receiver uses the same active phased array device as employed at the transmitter. The beamformer is configured in the receive (Rx) mode, employing a first-stage low noise amplifier (LNA) in the RF front-end, having a gain of 13 dB per branch and an overall noise figure (NF) of 14 dB, which is a relatively high NF [27]. Like the Tx-end, the phase shifters in the beamformer at the Rx-end are calibrated for maxima along the broadside direction. To obtain sufficient overall amplification, a second stage LNA manufactured by Mini-Cicruits [28], having a gain of 22 dB and NF 2.38 dB at 28 GHz, is cascaded after the receive beamformer. After the second LNA, a BPF [26] identical to the one at the Tx-end is employed to filter out harmonics generated by the combined Rx-end beamformer and second-stage LNA as well as LO leakage from the following down conversion unit (UD-Box).

Once the signal is downconverted to IF (2.52 GHz), a third stage of amplification is employed using a Mini-Circuit amplifier [29] having a gain of 20 dB and an NF of 1.4 dB. The purpose of the IF amplifier is to ensure the signal fully occupies the entire ADC dynamic range at low received power levels. In the experimental testbed, the ADC function was provided by a LeCroy Wavemaster 813Zi-A digital oscilloscope with an analog bandwidth of 13 GHz and 8-bit resolution. An BPF is inserted after the IF amplifier to suppress any image signals, LO leakage towards the IF, and other spurious signals that may be present. The -3 dB bandwidth of the IF BPF is

≈80 MHz (from 2.485 GHz - 2.565 GHz) with a minimum insertion loss of 1.3 dB at 2.53 GHz [30]. The output from the IF BPF is fed to the oscilloscope for direct IF sampling. The oscilloscope sensitivity was manually adjusted to ensure the received signal occupied the entire 8-bit resolution.

The digital back-end of the direct IF sampling receiver is realized using a NI-PXIe-8135 embedded controller where the sampled signal from the oscilloscope is digitally down-converted (DDC), consisting of digital numerically controlled oscillators (NCOs) followed by low-pass filters to extract the desired baseband IQ signal. The resulting IQ stream is processed by LabView's LTE Application Framework to recover the downlink physical shared channel (DPSCH) data as well as provide SNR, EVM and BLER measurements.

III. Experimental Results

The direct IF sampling receiver is characterized in an anechoic chamber over a 140 cm OTA wireless link at 28 GHz, as shown in Fig. 2. A 20 MHz LTE signal is employed as a baseband signal using modulation and coding scheme MCS9, which corresponds to QPSK digital modulation. The signal passes through the RF front-end as per the schematic provided in Fig.1 and is then made available for direct IF sampling at the 13 GHz inputs of the LeCroy WaveMaster oscilloscope. The receiver performance is characterized in terms of received SNR, EVM, and system BLER at sampling frequencies of 10 GSa/s (for the Nyquist sampling benchmark) and at 250 MSa/s, 500 MSa/s, 1 GSa/s and 2.5 GSa/s (for the subsampling cases). Although a theoretical 5.04 GSa/s sampling frequency could be used for the Nyquist sampling benchmark, 10 GSa/s was used as it is the lowest available rate that can be set on the oscilloscope for a 2.52 GHz IF.

The measured SNR for the direct IF sampling receiver is shown in Fig. 3 for different sampling frequencies. The SNRs are plotted against the received signal power level as measured at the input of the oscilloscope. A variation in the received power at the input of the oscilloscope can be achieved in different ways, for example, by inserting a variable attenuator in either the transmit or receive RF chains or by varying the baseband signal transmit power at the LabView-based LTE Application Framework running on the NI PXIe 8135 controller. The latter approach was adopted in the experimental testbed. Fig. 3 shows that as the received signal power at the input of the oscilloscope increased from -80 dBm to -60 dBm, an almost proportional increase in the SNR occurred. On average, a difference of ≈4.5 dB is observed between the SNR for a sampling rate of 10 GSa/s and 250 MSa/s, which reduces to about 3dB when compared with the 500 MSa/s and a further reduction with a difference of about 2 dB when compared with the sampling rate of 1 GSa/s.

The measured EVM versus received signal power for Nyquist and sub-Nyquist sampling are shown in Fig. 4. In the Nyquist sampling case (sampling at 10 GSa/s), the EVM increases from 6.9% to 38.6% when the received signal power decreases from -60 dBm to -80 dBm. For sub-Nyquist sampling at 250 MSa/s, the EVM increases from 13.86% (at a

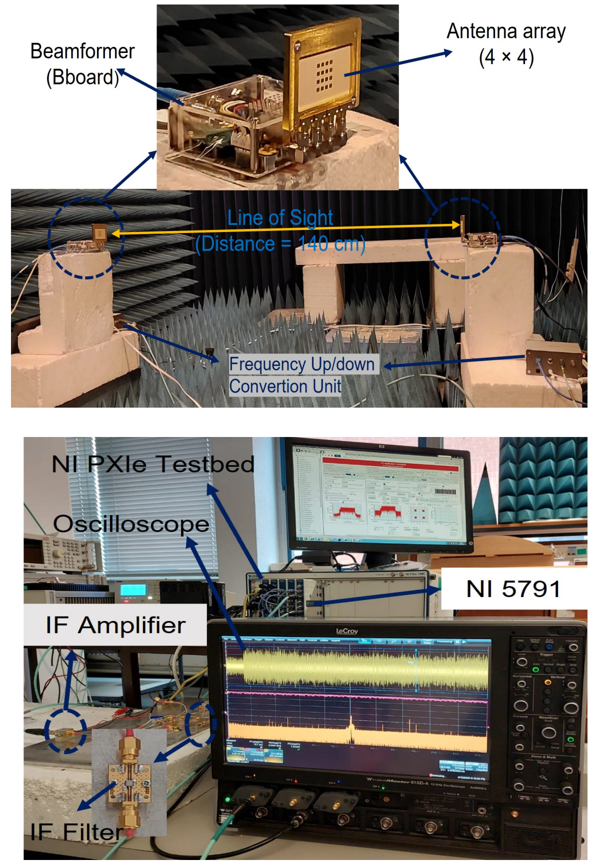

[] []

Fig. 2: HWIL SDR testbed (a) mm-wave chamber configuration (b) IF equipment and components.

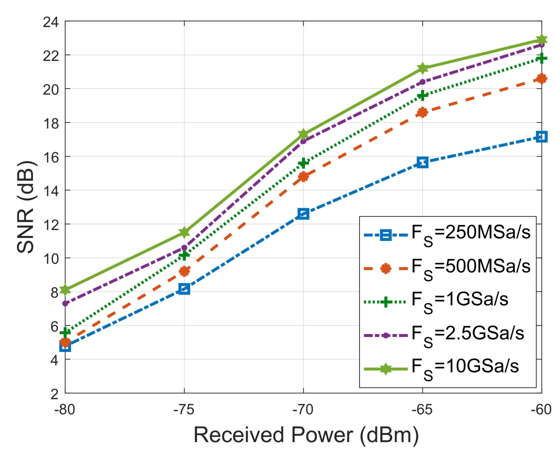

Fig. 3: Measured SNR against received input power at ADC.

received power of -60 dBm) to 57.66% (at received power of -80 dBm). Similar to SNR, an improvement in the EVM can be noted when the subsampling frequency is increased from 250 MSa/s to 2.5 Ga/S. According to the 3GPP standards, the target EVM of 17.5% for QPSK modulation would be realized at about $\{-73, -71, -70, -69, -66\}$ dBm received power corresponding to sampling rates of $\{10, 2.5, 1, 0.5, 0.25\}$ GSa/s, respectively. Importantly, the EVMs for sampling rates down to

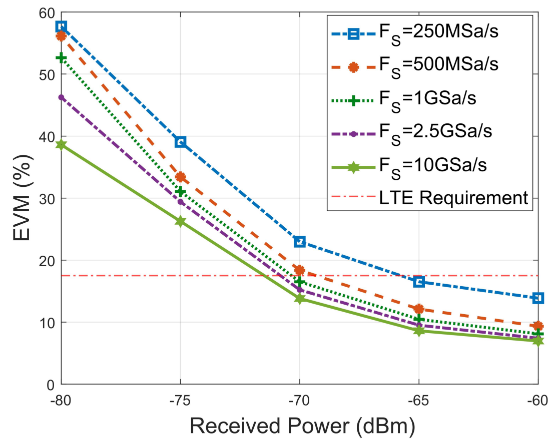

Fig. 4: Measured EVM against received input power at ADC.

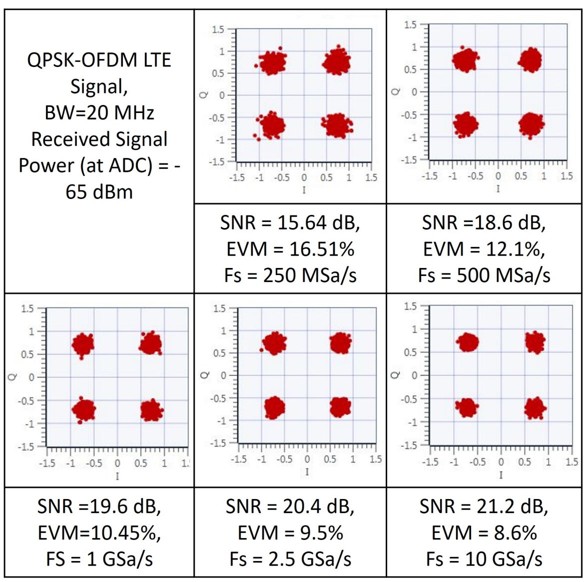

Fig. 5: Measured constellations for various sampling frequencies.

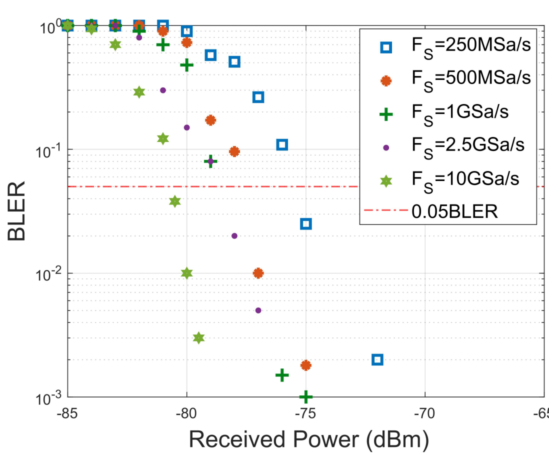

Fig. 6: Measured BLER against received input power at ADC.

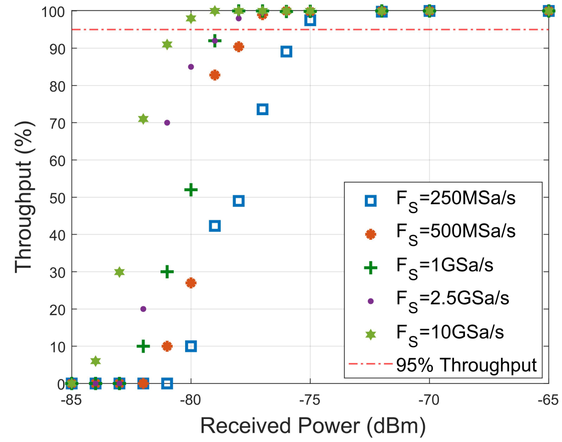

Fig. 7: Measured throughput against received input power at ADC.

TABLE I: Power penalty (loss in dB) compared to the Nyquist sampling at 10 GSa/s

Sampling Frequency	Power Penalty (dB) for a target EVM of 17.5%	Power Penalty (dB) for a BLER of $\leq 5\%$
250 MSa/s	5.5	5.5
500 MSa/s	3.0	3.5
1 GSa/s	2.0	2.5
2.5GSa/s	1.5	2.0

500 MSa/s converge in the high received signal power regime suggesting that a least sampling rate of 500 MSa/s should be used. Fig 5 depicts the measured QPSK constellation at the received power of -65 dBm where both the Nyquist and sub-Nyquist sampling cases meet the target EVM for the LTE signal, indicating that the received signal is of high quality (i.e., zero BLER).

The measured system BLER versus received signal power for the aforementioned testbed conditions is shown in Fig. 6 for different sampling rates of the oscilloscope. For 3GPP standards compliance, a BLER of 5% is targeted. From the curves in Fig. 6 this 5% target is reached at about $\{-81, -79, -79, -78, -76\}$ dBm received power corresponding to sampling rates of $\{10, 2.5, 1, 0.5, 0.25\}$ GSa/s, respectively. Importantly, these operating BLER targets correspond to EVMs of approximately 40% demonstrating the error resilience of the LTE turbo code. Also, the BLER trends support the observation from the EVM trends that a least sampling rate of 500 MSa/s could be adopted for the system under test. For these BLER measurements, at least 300 transport blocks were sent per data point. Finally, Fig. 7 plots normalized throughput, calculated as $100 \times (1 - BLER)$, versus received signal power with the sampling rate as a parameter. Hence, the throughput trends reflect the same trends observed for BLER measurements. For MCS9 the maximum raw data rate is 15.84 Mbit/s since a 1584 bits transport block size is used per 1ms transmission time interval. As the LTE Application Framework applies a channel coding rate of 0.66 for MCS9, the effective spectral efficiency is about 0.52 bit/s/Hz.

The power penalty (loss in dB) when a subsampling technique is employed over the baseline Nyquist sampling frequency of 10 GSa/s, is provided in Table I. Comparing direct IF sampling at 500 MSa/s to Nyquist sampling at 10 GSa/s, the 3 dB degradation in received signal power and, therefore, sensitivity is mainly due to the RF noise folding and increased in-band digital noise level. The relatively "good" performance of the subsampling receiver is attributable to the employed testbed's stringent filtering modules, particularly the IF filter that effectively mitigates the impact of noise folding. With a high out-of-band rejection ratio, the IF filter suppresses the spurious signal to a significant extent, which improves further the receiver performance, particularly for the subsampling scenario. A more detailed mathematical analysis of these effects, which is beyond the scope of this paper, will be carried out in the authors' future work.

The demonstration confirms the efficacy of a direct IF subsampling receiver for mm-wave communications systems. The direct IF sampling receiver incorporates the positive aspects of homodyne and superheterodyne (multi-stage RF down conversion) receivers. Direct sampling of high IF signals eliminates DC offset and low-frequency noise. It also serves the purpose of keeping the sampling frequency low, which, in practical receivers, results in the ADCs, the most power-hungry module in the RF chain, consuming less energy.

IV. Conclusion

Experimental implementation of a direct IF sampling receiver for a SISO OTA communication link in the 5G 28 GHz FR2 band has been carried out using an HWIL testbed. The SNR, EVM, BLER and throughput performance of the system is evaluated employing both Nyquist and sub-Nyquist sampling rates at an IF of 2.52 GHz. For a QPSK-modulated LTE signal subsampled at 500 MSa/s over a 10 GSa/s Nyquist sampling benchmark, a small SNR penalty of 3 dB at 5% BLER was recorded. The results demonstrate that the direct IF subsampling receiver is a suitable candidate for the 5G mm-wave wireless communication systems by both reducing receiver complexity and power consumption.

Acknowledgment

This work was supported by the UK Engineering and Physical Sciences Research Council, grant number EP/S008101/1.

References

[1] A. Gupta and R. K. Jha, "A Survey of 5G Networks: Architecture and Emerging Technologies," *IEEE Access*, vol. 3, pp. 1206–1232, 2015.

[2] M. Shafi, A. F. Molisch, P. J. Smith, T. Haustein, P. Zhu, P. De Silva, F. Tufvesson, A. Benjebbour, and G. Wunder, "5G: A Tutorial Overview of Standards, Trials, Challenges, Deployment, and Practice," *IEEE Journal on Selected Areas in Communications*, vol. 35, no. 6, pp. 1201–1221, 2017.

[3] S. Bronckers, A. Roc'h, and B. Smolders, "Wireless Receiver Architectures Towards 5G: Where Are We?," *IEEE Circuits and Systems Magazine*, vol. 17, no. 3, pp. 6–16, 2017.

[4] J. Moghaddasi and K. Wu, "Multifunction, Multiband, and Multimode Wireless Receivers: A Path Toward the Future," *IEEE Microwave Magazine*, vol. 21, no. 12, pp. 104–125, 2020.

[5] A. Arbi and T. O'Farrell, "Energy Efficiency in 5G Access Networks: Small Cell Densification and High Order Sectorisation," in *2015 IEEE International Conference on Communication Workshop (ICCW)*, pp. 2806–2811, 2015.

[6] S. Henthorn, T. O'Farrell, M. R. Anbiyaei, and K. L. Ford, "Concurrent Multiband Direct RF Sampling Receivers," *IEEE Transactions on Wireless Communications*, vol. 22, no. 1, pp. 550–562, 2023.

[7] S. Henthorn, T. O'Farrell, S. Asif, M. R. Anbiyaei, and K. Ford, "Tri-band Single Chain Radio Receiver for Concurrent Radio," in *2020 2nd 6G Wireless Summit (6G SUMMIT)*, pp. 1–5, 2020.

[8] J. Mitola, "The software radio architecture," *IEEE Communications Magazine*, vol. 33, no. 5, pp. 26–38, 1995.

[9] R. Singh, Q. Bai, T. O'Farrell, K. L. Ford, and R. J. Langley, "Concurrent, Tunable, Multi-Band, Single Chain Radio Receivers for 5G RANs," in *2017 IEEE 85th Vehicular Technology Conference (VTC Spring)*, pp. 1–5, 2017.

[10] T. O'Farrell, R. Singh, Q. Bai, K. L. Ford, R. Langley, M. Beach, E. Arabi, C. Gamlath, and K. A. Morris, "Tunable, Concurrent Multi-band, Single Chain Radio Architecture for Low Energy 5G-RANs," in *2017 15th International Symposium on Modeling and Optimization in Mobile, Ad Hoc, and Wireless Networks (WiOpt)*, pp. 1–6, 2017.

[11] A. A. Abidi, "The Path to the Software-Defined Radio Receiver," *IEEE Journal of Solid-State Circuits*, vol. 42, no. 5, pp. 954–966, 2007.

[12] "Analog devices AD9213." https://www.analog.com/en/products/ad9213.

[13] "Texas Instruments ADC12DJ5200RF." https://www.ti.com/product/ADC12DJ5200RF.

[14] S. Norsworthy, "RF Data Donversion for Software Defined Radios," in *2019 IEEE 20th Wireless and Microwave Technology Conference (WAMICON)*, pp. 1–4, 2019.

[15] D. Siafarikas and J. L. Volakis, "Toward Direct RF Sampling: Implications for Digital Communications," *IEEE Microwave Magazine*, vol. 21, no. 9, pp. 43–52, 2020.

[16] R. Barrak, A. Ghazel, and F. Ghannouchi, "Optimized Multistandard RF Subsampling Receiver Architecture," *IEEE Transactions on Wireless Communications*, vol. 8, no. 6, pp. 2901–2909, 2009.

[17] R. Fagan, F. C. Robey, and L. Miller, "Phased Array Radar Cost Reduction Through the Use of Commercial RF Systems on a Chip," in *2018 IEEE Radar Conference (RadarConf18)*, pp. 0935–0939, 2018.

[18] B. Farley, J. McGrath, and C. Erdmann, "An All-Programmable 16-nm RFSoC for Digital-RF Communications," *IEEE Micro*, vol. 38, no. 2, pp. 61–71, 2018.

[19] A. Collins, "All programmable RF-sampling solutions," *Xilinx White Paper*, 2017.

[20] B. Schweizer, A. Grathwohl, G. Rossi, P. Hinz, C. Knill, S. Stephany, H. J. Ng, and C. Waldschmidt, "The Fairy Tale of Simple All-Digital Radars: How to Deal With 100 Gbit/s of a Digital Millimeter-Wave MIMO Radar on an FPGA [Application Notes]," *IEEE Microwave Magazine*, vol. 22, no. 7, pp. 66–76, 2021.

[21] S. Pulipati, V. Ariyarathna, M. R. Khan, S. Bhardwaj, and A. Madanayake, "Aperture-Array and Lens+FPA Multi-Beam Digital Receivers at 28 GHz on Xilinx ZCU 1275 RF SoC," in *2020 IEEE/MTT-S International Microwave Symposium (IMS)*, pp. 555–558, 2020.

[22] N. Suematsu, "Direct Digital RF Technology - Challenges for Beyond Nyquist Frequency Range," in *2018 IEEE International Symposium on Radio-Frequency Integration Technology (RFIT)*, pp. 1–3, 2018.

[23] T. Furuichi, Y. Gui, M. Motoyoshi, S. Kameda, and N. Suematsu, "28 ghz band direct rf undersampling broadband receiver for ka-band hts on-board unit," in *2019 12th Global Symposium on Millimeter Waves (GSMM)*, pp. 56–58, 2019.

[24] "National Instruments 5791R User Manual and Specifications." https://www.ni.com/docs/en-US/bundle/373845d/resource/373845d.pdf.

[25] "TMYTEK Frequency Converter Unit." https://www.tmytek.com/products/frequency-converters/udbox5g.

[26] "Mini-Circuits Bandpass Filter Datasheet." https://https://www.minicircuits.com/pdfs/ZVBP-28000-K+.pdf.

[27] "TMYTEK Beamformer Specifications." https://www.tmytek.com/products/beamformers/bboard.

[28] "Mini-Circuits Low Noise Amplifier Datasheet." //https://www.minicircuits.com/pdfs/ZVE-323LN-K+.pdf.

[29] "Mini-Circuits Low Noise Amplifier Datasheet." //https://www.minicircuits.com/pdfs/ZX60-83LN12+.pdf.

[30] "TAI-SAW Technology Filter Specifications." https://www.taisaw.com/upload/product/TA1683A$\%$20_Rev.1.0_.pdf.